Phase decomposition and chemical inhomogeneity in $Nd_{2-x}Ce_xCuO_{4\pm\delta}$

P. K. Mang,[1] S. Larochelle,[2,*] A. Mehta,[3] O. P. Vajk,[2,†] A. S. Erickson,[1] L. Lu,[1] W. J. L. Buyers,[4] A. F. Marshall,[5] K. Prokes,[6] and M. Greven[1,3]

[1]*Department of Applied Physics, Stanford University, Stanford, California 94305, USA*

[2]*Department of Physics, Stanford University, Stanford, California 94305, USA*

[3]*Stanford Synchrotron Radiation Laboratory, Stanford University, Stanford, California 94309, USA*

[4]*National Research Council, Neutron Program for Materials Research, Chalk River Laboratories, Chalk River, Ontario K0J 1J0, Canada*

[5]*T. H. Geballe Laboratory for Advanced Materials, Stanford University, Stanford, California 94305, USA*

[6]*Hahn-Meitner-Institut, Glienicker Str. 100, Berlin D-14109, Germany*

(Received 20 December 2003; revised manuscript received 9 March 2004; published 17 September 2004)

Extensive x-ray and neutron scattering experiments and additional transmission electron microscopy results reveal the partial decomposition of $Nd_{2-x}Ce_xCuO_{4\pm\delta}$ (NCCO) in a low-oxygen-fugacity environment such as that typically realized during the annealing process required to create a superconducting state. Unlike a typical situation in which a disordered secondary phase results in diffuse powder scattering, a serendipitous match between the in-plane lattice constant of NCCO and the lattice constant of one of the decomposition products, $(Nd,Ce)_2O_3$, causes the secondary phase to form an oriented, quasi-two-dimensional epitaxial structure. Consequently, diffraction peaks from the secondary phase appear at rational positions $(H,K,0)$ in the reciprocal space of NCCO. Additionally, because of neodymium paramagnetism, the application of a magnetic field increases the low-temperature intensity observed at these positions via neutron scattering. Such effects may mimic the formation of a structural superlattice or the strengthening of antiferromagnetic order of NCCO, but the intrinsic mechanism may be identified through careful and systematic experimentation. For typical reduction conditions, the $(Nd,Ce)_2O_3$ volume fraction is approximately 1%, and the secondary-phase layers exhibit long-range order parallel to the NCCO CuO_2 sheets and have a typical thickness of approximately 100 Å. The presence of the secondary phase should also be taken into account in the analysis of other experiments on NCCO, such as transport measurements.

DOI: 10.1103/PhysRevB.70.094507 PACS number(s): 74.72.Jt, 75.25.+z, 75.50.Ee, 61.10.Nz

I. INTRODUCTION

One of the central challenges in the field of correlated-electron materials is to understand the nature of competing or coexisting ground states of the high-temperature superconductors. These materials are charge-carrier-doped antiferromagnetic Mott insulators, and both static and dynamic antiferromagnetic correlations have been found to exist even in the superconducting state. Recent neutron scattering experiments on the hole-doped material $La_{2-x}Sr_xCuO_4$ have revealed an increase of the (incommensurate) low-energy antiferromagnetic response in an applied magnetic field,[1–4] which has been argued to indicate that the superconductor is in the vicinity of a bulk quantum phase transition to a state with microscopic coexistence of superconducting and spin-density-wave orders.[5] Unfortunately, the low-temperature upper critical field H_{c2} of hole-doped materials is too large to be accessible at neutron scattering facilities. The electron-doped materials, typified by $Nd_{2-x}Ce_xCuO_{4\pm\delta}$ (NCCO), have much lower values of H_{c2} ($\leqslant 12$ T for $\mathbf{H}\|[0,0,1]$),[6,7] and thus, in principle, offer the opportunity to access the nonsuperconducting ground state.

Since their discovery[8] in 1989, NCCO and related electron-doped superconductors have presented a number of experimental challenges to understanding the physics of the system. Foremost among those is that, unlike other cationically substituted systems, NCCO is not superconducting in its as-grown state. Instead, a post-growth annealing procedure, typically consisting of a high-temperature exposure to an argon or nitrogen atmosphere, is needed to induce superconductivity. Ostensibly, this is necessary to remove excess oxygen impurities, but the exact effect of the procedure is yet unclear.

Using x-ray and neutron diffraction as well as transmission electron microscopy, we find that an unintended byproduct of this reduction step is to partially decompose NCCO, forming layers of oriented epitaxial neodymium cerium oxide, $(Nd,Ce)_2O_3$. Because of a serendipitous match of lattice constants between NCCO and this secondary phase, certain $(Nd,Ce)_2O_3$ diffraction peaks are commensurate with the NCCO reciprocal lattice. Upon application of a magnetic field, $(Nd,Ce)_2O_3$ exhibits a paramagnetic response even at a temperature of 1.9 K. Knowledge about the structural and magnetic properties of the secondary phase is essential in order to separate intrinsic properties from extrinsic effects when investigating the connection between magnetism and superconductivity in NCCO. Specifically, the extensive data we present are inconsistent with the notion of a field-induced quantum phase transition from a superconducting to an antiferromagnetic state[9–13] and have a more prosaic origin—a paramagnetic impurity phase. Consequently, the question of genuine magnetic field effects in NCCO remains unresolved, and it may well be that the field-induced ground state does not exhibit long-range magnetic order. A brief summary of

 ©2004 The American Physical Society

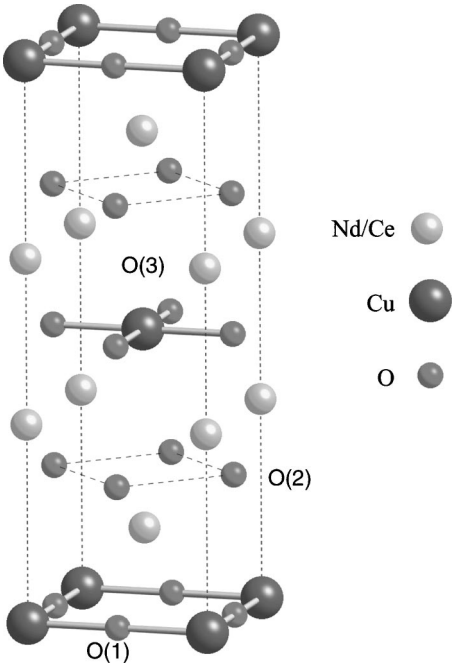

FIG. 1. Unit cell of $Nd_{2-x}Ce_xCuO_{4\pm\delta}$. The structure is of $I4/mmm$ (No. 139) symmetry and tetragonal at all temperatures. For the undoped compound, the room-temperature lattice constants are $a \approx 3.94$ Å and $c \approx 12.1$ Å. The apical oxygen site O(3) is nominally vacant.

some of our results was published recently.[14]

This paper is organized as follows: after a discussion of the NCCO crystal structure (Sec. II) and of some experimental details (Sec. III), we describe the oxygen-reduction procedure that is required to render NCCO superconducting in the cerium-doping regime $0.13 < x < 0.20$ (Sec. IV). We then summarize previous results for rare earth oxides of the form R_2O_3 (Sec. V) and proceed to present our structural x-ray diffraction (Sec. VI) and transition electron microscopy (Sec. VII) work. Finally, we present detailed magnetic neutron scattering results of the magnetic field effects observed in reduced NCCO in Sec. VIII, and discuss our results together with previous work in Sec. IX. A summary is given in Sec. X.

II. STRUCTURE

$Nd_{2-x}Ce_xCuO_{4\pm\delta}$ crystallizes into a modified form of the body-centered tetragonal K_2NiF_4 structure found for other single-layer cuprate superconductors.[15] The structure is tetragonal at all temperatures and is shown schematically in Fig. 1. What is unique about NCCO vis-à-vis other single-layer cuprates is the nominal absence of apical oxygen atoms.[16–18] Instead, the out-of-plane oxygen atoms are located directly above and below the in-plane oxygens. This is known as the T' structure. In the more common T structure, oxygen atoms are present both above and below the copper site, forming an octahedron as in hole-doped $La_{2-x}Sr_xCuO_4$. There exists a third, hybrid structure (T^*), in which one of the apical sites is occupied and the other is vacant.

A key characteristic of the T' structure is the square-planar coordination of copper. Apical oxygen disorder has been put forward to explain why a reduction procedure is necessary to produce a superconducting phase in NCCO. According to that argument, the apical sites are randomly occupied by a small fraction δ of interstitial oxygen in as-grown crystals. In addition to changing the carrier density in the CuO_2 sheets, this produces a random pinning potential for the doped electrons which prohibits superconductivity. The purpose of the reduction procedure is to remove the interstitial oxygen, after which superconductivity may occur. Unfortunately, this simple picture has been extremely difficult to verify. Generally, nonstoichiometric oxide materials can be stable for a wide range of oxygen concentrations[19] and the precise starting composition and oxygen site occupancies are typically unknown.

Based on single-crystal neutron diffraction studies, Radaelli *et al.*[15] concluded that the apical O(3) site has an occupancy of ~ 0.1 at the position $[0,0,0.2]$ in as-grown $Nd_2CuO_{4\pm\delta}$. In reduced samples, the occupancy was found to be lowered to ~ 0.04. The authors also reported less than full occupancy at both the O(1) in-plane and O(2) out-of-plane sites, and these were not seen to vary beyond one standard deviation with reduction. Further neutron diffraction experiments on NCCO ($x=0.15$) showed a smaller amount of apical oxygen (~ 0.06) in the as-grown state, which is lowered to ~ 0.04 upon reduction.[20] The diffraction data indicate that interstitial oxygen is probably present at the apical site in amounts negatively correlated with the cerium doping level. Presumably, this anticorrelation is a consequence of the contraction of the c-lattice constant,[21] which permits a decreasing number of interstitials at higher doping. The occupancies of the other two oxygen sites were found to be similar to the undoped case ($x=0$). Because of the measured incomplete occupancy of the O(1) and O(2) sites, even with the presence of additional interstitial oxygen, summation over the oxygen site occupancies was found to give stoichiometries of 3.97(4) and 3.95(3) for as-grown undoped ($x=0$) and doped ($x=0.15$) compounds, respectively. This suggests that as-grown crystals may, in fact, be oxygen deficient. In any case, the amount of oxygen removed from the various sites, particularly in the superconducting composition range ($0.13 < x < 0.20$), is near the detection limit of neutron diffraction, further confounding efforts to understand the exact effect of the reduction step. A Mössbauer study on ^{57}Co substituted NCCO gave evidence for the presence of apical oxygens even after reduction.[22] Other methods of measuring the oxygen content, such as thermogravimetric analysis and titration techniques, typically are not site specific.

III. EXPERIMENT

All crystals used in this study were grown in the T.H. Geballe Laboratory for Advanced Materials at Stanford University (Stanford, CA) using the traveling-solvent floating-zone technique. As grown, NCCO exhibits strong spin correlations in the paramagnetic phase and long-range antiferromagnetic order at low temperature. The crystals were grown in 4 atm of O_2, which results in samples with

TABLE I. Table of the reduced samples studied, with cerium concentration, superconducting transition temperature (onset), reduction conditions, experimental probe used, approximate $(Nd,Ce)_2O_3$ volume fraction (VF) (Ref. 27), as well as estimates of the typical thickness along [0,0,1] of the $(Nd,Ce)_2O_3$ secondary phase.

Sample	x	T_c(K)	Reduction condition	Probe	$(Nd,Ce)_2O_3$ VF	Thickness (Å)
NCCO0[a]	0	-	890°C/11 h/Ar	X-rays	0.02%	-
NCCO10[b]	0.10	-	960°C/20 h/Ar;500°C/20 h/O_2	Neutrons	2%	115
NCCO14LR[c]	0.14	-	960°C/1 h/Ar	X-rays	0.02%	60
NCCO14	0.14	24	960°C/20 h/Ar;500°C/20 h/O_2	X-rays	1%	80
Core/Shell[d]	0.14	24	970°C/10 h/Ar;500°C/20 h/O_2	Neutrons, X-rays	0.5%	80
NCCO16	0.16	24	960°C/20 h/Ar;500°C/20 h/O_2	TEM	2%	60
NCCO18	0.18	20	960°C/10 h/Ar	Neutrons	0.5%	160

[a]Insufficient data to determine thickness.
[b]Thickness determined from magnetic measurements of the $(Nd,Ce)_2O_3$ secondary phase (from fits shown in Fig. 13).
[c]T_c was not measured for this sample.
[d]Volume fraction and thickness from x-ray diffraction on a small piece of crystal, prior to separating the sample into core/shell pieces.

relatively high oxygen content and Néel temperatures.[23] Cerium concentrations of the grown boules were verified by inductively coupled plasma (ICP) analysis. The cerium solubility limit is close to $x=0.18$. With the exception of the $x=0.18$ sample, for which ICP carried out on different crystal pieces indicated a somewhat inhomogeneous Ce distribution of ±0.02, the Ce concentrations were found to be uniform. "Optimal" doping, with $T_c=24-25$ K (onset), is achieved for suitable reduction conditions and cerium concentrations of $x=0.14-0.16$. Details pertaining to the samples used in the present study are listed in Table I.

The room-temperature in-plane lattice constant of NCCO, $a\approx 3.94$ Å, increases very slightly with doping, by about 0.3%. The c-lattice constant decreases by about 1% with cerium doping, from 12.16 Å in the undoped material to 12.05 Å for $x=0.18$. In this paper, we will index reflections according to two different schemes. One is based on the tetragonal unit cell of NCCO. The other is based on the cubic unit cell of Nd_2O_3.[24] Reflections indexed according to the latter scheme will be marked by the subscript "c."

X-ray diffraction data were taken in reflection mode at beam line 7-2 of the Stanford Synchrotron Radiation Laboratory. The beam was monochromatized at 14 keV from a wiggler spectrum using a Si(111) double-crystal monochromator. The x-ray attenuation length was approximately 20 μm. Neutron diffraction data were taken using the spectrometers BT2 at the National Institute of Standards and Technology (NIST) Center for Neutron Research (Gaithersburg, MD, USA), E4 at the Hahn-Meitner-Institut (Berlin, Germany), and N5 at Chalk River Laboratories (Chalk River, Canada). Transmission electron microscope (TEM) images were taken with a FEI CM20 FEG-TEM instrument in the T.H. Geballe Laboratory for Advanced Materials at Stanford University.

IV. REDUCTION

Regardless of the microscopic effects of the reduction step, it is clear that such a procedure is necessary to induce superconductivity. Kim and Gaskell[26] investigated the stability field of $Nd_{1.85}Ce_{0.15}CuO_{4\pm\delta}$ as a function of temperature and oxygen partial pressure. They determined that $Nd_{2-x}Ce_xCuO_{4\pm\delta}$ is unstable toward decomposition into $Nd_2O_3+NdCeO_{3.5}+Cu_2O$ under sufficiently severe reducing conditions. Interestingly, they found that superconductivity only appears for conditions in which CuO is converted to Cu_2O in the binary system Cu-O, and that the superconducting transition temperature monotonically increases as one approaches the phase decomposition boundary during the reduction process.

Our own studies indicate that the resultant superconducting state is highly dependent on the parameters used in the reduction process. Figure 2 demonstrates the sensitivity of the transition temperature and the magnetic susceptibility on the annealing conditions. In order to find optimal conditions, that is, conditions that result in a sample with the highest T_c, we employed a tube furnace in which the sample was completely enclosed in a quartz tube and could be rapidly heated and quenched in a controlled atmosphere. We used high-purity argon gas containing less than 0.5 ppm O_2. A series of small samples of approximately 400 mg were cut from a single-crystal boule of NCCO ($x=0.14$) and were exposed to an argon environment at different temperatures and for varying durations.[25] A measurable change in sample mass, ranging from 0.1 to 0.3% was observed, corresponding to a change in oxygen content on the order of $\delta=0.04$. Samples annealed at 990°C and above suffered severe damage and eventually decomposed. Examination of the reduced samples revealed that the interior was less damaged than the exterior. We found the optimal annealing conditions for $x=0.14$ to be 970°C for 10 h in argon, followed by 500°C for 20 h in oxygen. In general, the additional low-temperature oxygen anneal tends to increase T_c by approximately 1 K. Other work[28] indicates the existence of two metastable phases for $x=0.15$, with values of T_c of 18 and 25 K. The higher-T_c samples were produced under conditions similar to ours, whereas the lower-T_c ones were created in a more benign reducing environment with an oxygen concentration of 1000 ppm.

The difference we observed between the interior and exterior regions of our samples suggests that, because of the

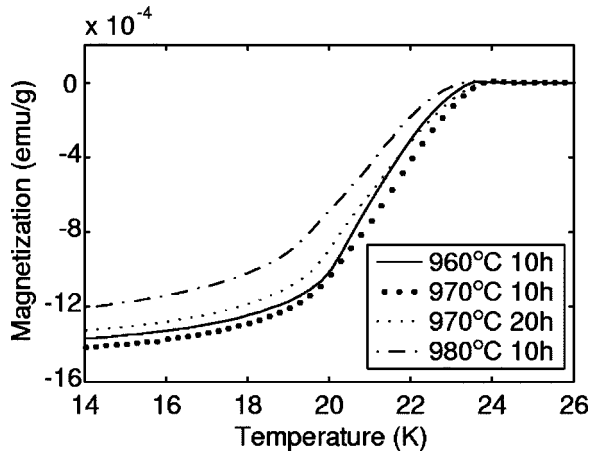

FIG. 2. AC magnetic susceptibility of $Nd_{1.86}Ce_{0.14}CuO_{4\pm\delta}$ crystals reduced in argon under various conditions. A subsequent low-temperature oxygen anneal raised the transition temperature by approximately 1 K (data not shown). The stated temperature was the temperature at the sample position. The control temperature of the tube furnace was measured by an external thermocouple, situated outside the quartz tube at the bottom of the sample chamber. There was a difference of ≈38 K between the control temperature and the (higher) sample temperature which was measured by a thermocouple placed directly above the sample inside the quartz tube (Ref. 25). Susceptibility measurements were performed in an AC excitation field of 0.02 Oe at 10000 Hz.

long time scale for oxygen diffusion, the resultant oxygen distribution in large reduced samples is not homogeneous. In order to test this proposition, we measured the magnetic intensity from the interior and exterior regions on the same sample. First, we reduced a cylindrical crystal boule ($x=0.14$) and cut it into two halves, perpendicular to the cylinder axis. One half was mechanically ground, which decreased the diameter from 4.2 to 3.2 mm and revealed the inner core of the crystal. The other half was cut lengthwise and the inner section was removed to create a hollow shell that was 1 mm thick. Mosaic scans through the (1/2,1/2,1) magnetic Bragg reflection were taken for both the core and the shell pieces and are compared in Fig. 3 to a scan previously made on the entire boule. The magnetic signal from the shell piece is an order of magnitude stronger than that of the core, but the averaged signal of the two contributions, weighted by the mass of each section, reproduces the signal of the whole sample. Due to the weakness of the signal, it is difficult to assess the exact onset of magnetic order in the core piece, but the Néel temperature ($T_N \sim 100$ K) does not likely differ by more than 20 K between the two. Remarkably, despite the large difference in the strength of the magnetic signal, no difference could be detected in the onset of superconductivity between the core and the shell piece. This suggests that the core is in some sense the better sample, since it has an equally high superconducting transition temperature and a weaker antiferromagnetic phase. Magnetic susceptibility experiments performed on pulverized pieces of the core and shell sample gave superconducting volume fractions of 10(5)%, but we note that it is difficult to obtain accurate estimates of superconducting volume fractions from such measurements.

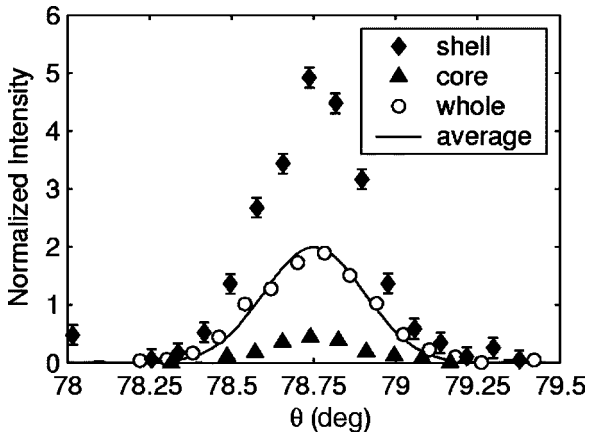

FIG. 3. Low-temperature neutron diffraction mosaic scans through the antiferromagnetic (1/2,1/2,1) peak for oxygen-reduced $x=0.14$ samples (Core/Shell; see Table I). Individual scans are shown for the outer shell, the inner core, and the whole crystal prior to division. The solid line represents a weighted average of the shell and core signals. Intensities were normalized by counting time, sample mass, and neutron flux. The data were taken at the NIST Center for Neutron Research (Gaithersburg, MD, USA).

It is possible that the reducing conditions employed are too severe and that they precipitate chemical decomposition that destroys superconductivity beyond a certain threshold. The core piece, protected by the shell, is less exposed to the severe reducing atmosphere. This is consistent with work by Brinkmann *et al.*[29] who reported an extended superconducting dome down to $x=0.04$ in $Pr_{2-x}Ce_xCuO_{4\pm\delta}$ when samples were subjected to a very high reduction temperature of 1080 °C, but protected from decomposition by being sandwiched between chemically homogeneous polycrystalline slabs.

V. RARE EARTH OXIDES

Rare earth elements form polymorphic sesquioxides of the form R_2O_3. There exist three low-temperature (A, B, and C) and two high-temperature (H and X) structural phases.[30] The preferred phase varies with rare earth ionic radius and temperature. In the case of Nd_2O_3, the trigonal A-modification is most commonly found. However, the cubic C-modification has also been observed. The cubic phase has the bixbyite structure with space group *Ia*3 (No. 206).[31,32] The unit cell is very large, with 32 rare earth ions occupying two different crystallographic sites, as shown schematically in Fig. 4. Because of the difficulty in preparing the cubic modification of Nd_2O_3 its magnetic structure is unknown, to the best of our knowledge. However, Moon *et al.*[24] studied the magnetic structures of Er_2O_3 and Yb_2O_3, which also possess the bixbyite crystal structure. The two systems were found to have Néel temperatures of $T_N=3.4$ and 2.3 K, respectively, and differing antiferromagnetic structures, each describable by four magnetic sublattices. Complex magnetic field effects were observed for Er_2O_3, but not reported in detail.

VI. STRUCTURAL X-RAY DIFFRACTION

Additional diffraction peaks in reduced samples of NCCO were observed previously by both electron[33] and neutron[28]

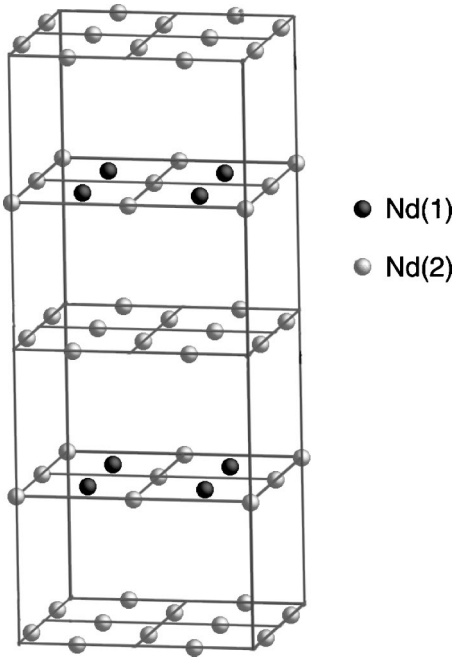

FIG. 4. Stylized Nd_2O_3 unit cell, modeled after Fig. 2 of Ref. 24. The unit cell is cubic, but the *c*-axis has been expanded and the oxygen atoms are omitted for clarity. There are two crystallographically distinct Nd sites; the ones in grey have C_2 site symmetry [Nd(2) sites] and the ones in black have C_{3i} symmetry [Nd(1) sites]. The C_2 atoms are displaced from the shown positions along one of the cell edges by about 1/30 of a unit cell.

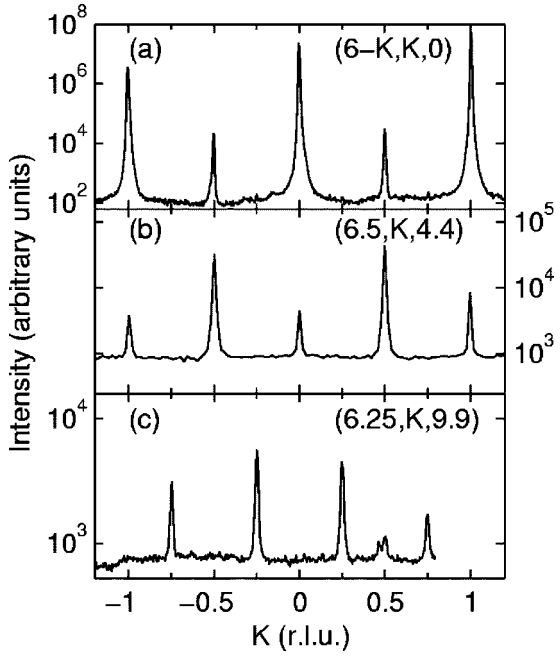

FIG. 5. X-ray diffraction data for a reduced $x=0.14$ sample (NCCO14; see Table I). The scans were taken at (a) 30 K, (b) 300 K, and (c) 7 K. Note the logarithmic intensity scale.

diffraction. These peaks were attributed, respectively, to the formation of an oxygen vacancy superstructure and to coherent atomic displacements. Using x-ray diffraction, we investigated the formation of additional peaks at two cerium concentrations: undoped ($x=0$) and optimally doped ($x=0.14$). Data for a lightly reduced $x=0.10$ sample (not shown) are consistent with the results presented here.

Diffraction peaks other than those expected from the $I4/mmm$ structure of NCCO were not observed in as-grown NCCO at any cerium concentration, but are present in all samples that have been subjected to a reduction treatment, including the undoped sample. The peaks appeared relatively early in the reduction process, and were observable in a sample that had been reduced for only one hour, compared to the duration of 10–20 h normally employed to obtain optimized superconducting properties. The samples exhibited varying degrees of diffuse scattering, examples of which will be given shortly. The sample with the sharpest additional peaks and the least diffuse scattering among all crystals studied with x-rays was an optimally doped NCCO ($x=0.14$) crystal, which we discuss first.

From Figs. 5 and 6, we identify three classes of peaks [besides those present in as-grown NCCO]. Figure 5(a) reveals both the anticipated Bragg peaks from the NCCO structure at integer *K* positions and an additional contribution at half-integer positions, such as (5.5,0.5,0). The latter are located at the same position in reciprocal space as the antiferromagnetic zone center, but are unconnected with magnetism in NCCO. Nonresonant x-ray scattering is only weakly sensitive to magnetism, and the observed peaks exist at room temperature, well above the magnetic ordering temperature. Figure 5(b) reveals a second set of half-integer peaks, such as (6.5,0,4.4), that occur when one in-plane index is an integer, and Fig. 5(c) shows a final set of peaks at quarter-integer positions, such as (6.25,0.25,9.9).

Although these peaks appear at rational *H* and *K* indices, they possess an unusual *L*-dependence. Careful examination

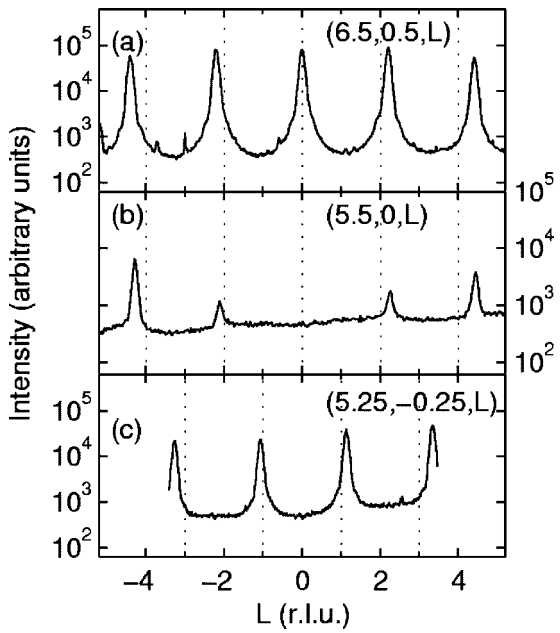

FIG. 6. Room-temperature scans perpendicular to the copper-oxygen plane for the same sample as in Fig. 5. Note the logarithmic intensity scale.

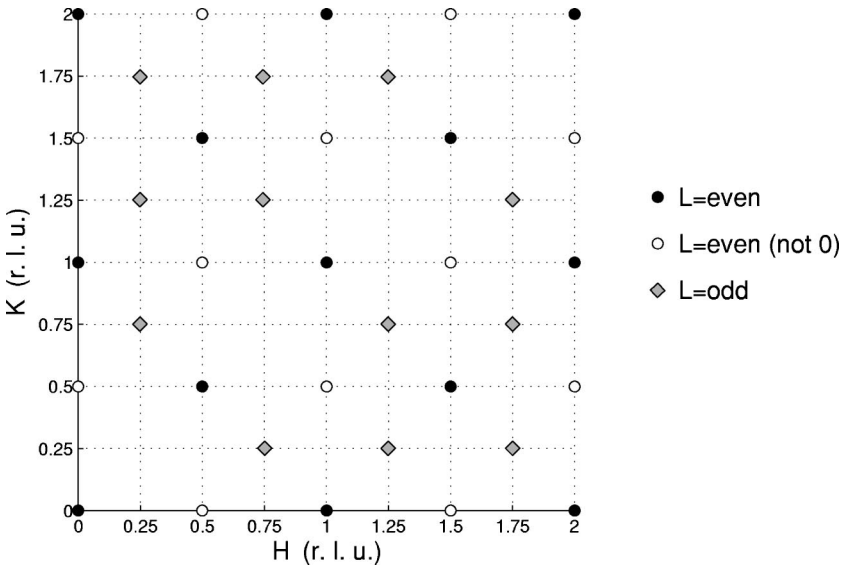

FIG. 7. Reciprocal space map indicating the $(Nd,Ce)_2O_3$ positions where peaks are observed in reduced samples of NCCO. L=even indicates that out-of-plane peaks are centered at even integer multiples of $L=\pm 1.1$: $L=\{0,\pm 2.2,\pm 4.4,\ldots\}$. L=even (not 0) implies the same, except that no peak is observed for $L=0$. L=odd indicates a third class of peaks that are centered at $L=\{\pm 1.1,\pm 3.3,\ldots\}$. Note that this map does not include the reciprocal space positions where scattering becomes allowed once the glide-plane symmetry of cubic $(Nd,Ce)_2O_3$ is broken, such as (0,0.5,0) and equivalent positions (see also Fig. 8).

of Fig. 6 reveals that, for these three classes of peaks, the incommensurability systematically increases along [0,0,1]. This is different from scattering due to a superstructure, in which case the incommensurability is constant for all Brillouin zones. The additional diffraction peaks have L indices of $\{0,\pm 1.1,\pm 2.2,\ldots\}$. This peculiar L-dependence suggests that these peaks are due to a secondary phase that is well oriented with the [0,0,1] surface of NCCO, and that the c-lattice constant is approximately 10% smaller than that of NCCO.

On the basis of this extensive survey of the positions of the additional peaks, we construct the map of reciprocal space of the secondary phase in Fig. 7. All the peaks on the map can be indexed by a unit cell with dimensions $(2\sqrt{2}a, 2\sqrt{2}a, c/1.1)$, where a and c refer to the lattice constants of the tetragonal NCCO unit cell. We find that this indexing is consistent with the presence of the bixbyite phase of $(Nd,Ce)_2O_3$. When a secondary phase bears no special relationship with the surrounding matrix, it often precipitates as randomly oriented polycrystalline inclusions. Such inclusions result in rings of scattering at constant momentum transfer, commonly referred to as powder rings. If, however, the arrangements of atoms in one (or more) of the lattice planes of the secondary phase closely match the atomic arrangements of a lattice plane of the host matrix, then a secondary phase may precipitate epitaxially onto the special plane of the host lattice. Such a match is present between the basal plane of the bixbyite phase of $(Nd,Ce)_2O_3$ (nominal lattice constant $a_c \approx 11.08$ Å) and the diagonal of the CuO_2 planes of NCCO, $2\sqrt{2}a$ ($\approx$11.14 Å). This nearly perfect (within $\approx$0.5%) match leads to the precipitation of thin "plates" of the secondary phase of $(Nd,Ce)_2O_3$ which are well oriented with the copper-oxygen planes of NCCO. As will be shown below, these secondary-phase plates extend only relatively few unit cells along [0,0,1], and hence are quasi-two-dimensional in nature. We note that the lattice constant a_c of the bulk bixbyite phase of Nd_2O_3 is indeed $\sim$10% smaller than the c-axis lattice constant of NCCO.

Based on a careful examination of the location of many of the secondary-phase peaks we find that the lattice parameter perpendicular to the epitaxial plane is 10.95(2) Å, whereas the in-plane lattice parameter is 11.14(2) Å. Therefore, the structural symmetry of the bixbyite secondary phase in reduced NCCO is no higher than tetragonal. Since the cubic space group $Ia3$ has no fourfold symmetry, the actual symmetry of the secondary-phase inclusions is most probably orthorhombic. We noticed that the tetragonal distortion of the epitaxial precipitates does not result in any significant change of the unit cell volume from the value of the bulk bixbyite phase of Nd_2O_3:[30] $(11.14\ \text{Å})^2 \times 10.95\ \text{Å} \approx (11.08\ \text{Å})^3 \approx a_c^3$.

Furthermore, there is evidence that the glide-plane symmetry present in the original space group ($Ia3$) is broken. In samples with relatively low volume fractions of the secondary phase, weak additional scattering was easily observed at positions forbidden by the glide-plane symmetry. Note the small peak at (6,0.5,0) [equivalent to $(13,11,0)_c$] in Fig. 8(b), a position forbidden by the glide-plane symmetry. This central peak has the same L-width as the two peaks at $(6,0.5,\pm 2.2)$, implying that the glide-plane symmetry is broken in all secondary-phase regions.

The lowered structural symmetry of the secondary phase further increases the complexity of the structure, and results in more than just two crystallographically (and most probably also magnetically) distinct rare earth sites. Consequently, it would not be surprising if the magnetic response of the secondary-phase inclusions was even more complex than that of bulk bixbyite rare earth oxides.

Strong diffuse scattering is responsible for what appear to be peaks at quarter-integer positions in Fig. 8(a). This intensity actually results from bisecting a rod of diffuse scattering that connects the quarter-integer peaks located above and below the scattering plane at $L=\pm 1.1$. The relative amount of diffuse scattering present in the two $x=0.14$ samples can be gauged by comparing Figs. 5(a) and 8(a) as well as Figs. 6(b) and 8(b).

The widths of the additional diffraction peaks are anisotropic with respect to the in-plane and out-of-plane directions. For example, while the in-plane half-width-at-half-maximum (HWHM) of the (5.5,0.5,2.2) peak ($\sim$0.0043

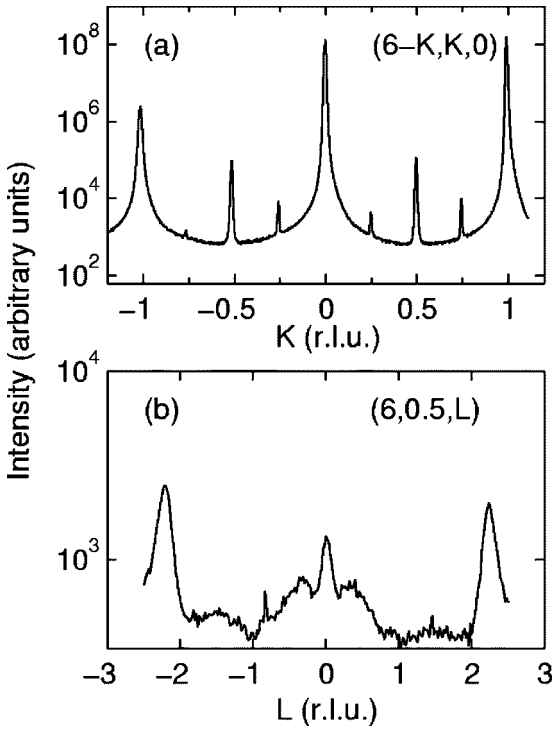

FIG. 8. Room-temperature scans for a lightly-reduced $x=0.14$ sample of NCCO (NCCO14LR; see Table I). (a) A cut across diffuse rods centered above and below the $L=0$ plane at $L=\pm 1.1$ results in the appearance of pseudopeaks at quarter positions that were not visible in Figs. 5 and 6. (b) Large amounts of diffuse scattering not seen in Fig. 6 culminating in a peak at $L=0$. This is evidence that the glide-plane symmetry of $(Nd,Ce)_2O_3$ is broken. Note the logarithmic intensity scale.

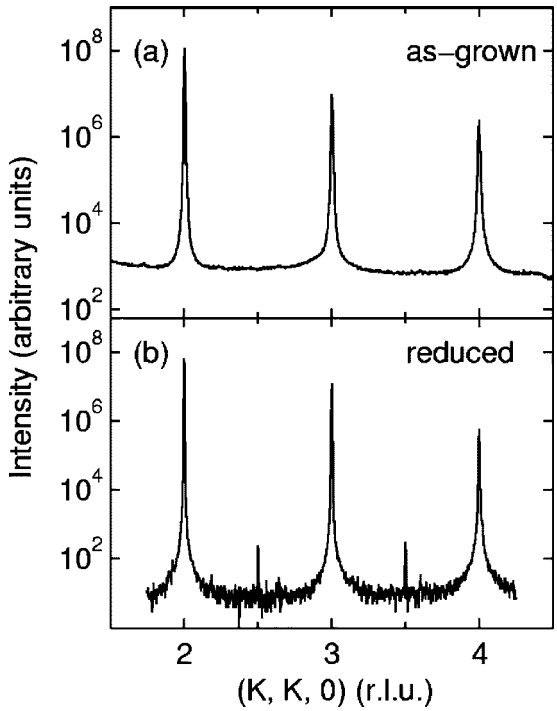

FIG. 9. Room-temperature scan along $(K,K,0)$ in an undoped sample (NCCO0; see Table I). (a) The sample is in its as-grown state and no scattering is visible at the half-integer positions. (b) After being reduced in flowing Ar at 890 °C for 11 h, new peaks appear at the half-integer positions. Note the logarithmic intensity scale.

r.l.u.) of sample NCCO14 is only slightly larger than that of the NCCO Bragg peaks, the width along the out-of-plane direction (~0.066 r.l.u.) is an order of magnitude larger. As discussed in more detail below, this implies a typical in-plane length of at least several hundred Å, but a thickness of only 80 Å. The typical thickness of the epitaxial layers of $(Nd,Ce)_2O_3$ can be estimated from the width of the diffraction peaks emanating from the secondary phase. Specifically, an estimate is provided by the full-width-at-half-maximum of the Fourier transform of a Gaussian peak, since the shape of our diffraction peaks is well described by a Gaussian function. This is calculated according to the formula $t=[2\ln(2)/\pi](c/w)$, where t is the thickness, c is the lattice constant of NCCO, and w is the HWHM of the diffraction peak in reciprocal lattice units.

The thickness of a thin film should normally be estimated from the formula for diffraction from an N-slit grating.[34] However, the N-slit formula implies the existence of secondary diffraction maxima (see, for example, Fig. 5 of Ref. 35) which we do not observe for $(Nd,Ce)_2O_3$ because there exists a distribution of layer thicknesses. We note that the Fourier transform of a Gaussian peak gives a result that is equivalent to the N-slit formula for large N.

In Fig. 9, we compare a scan along $(K,K,0)$ for an undoped sample ($x=0$) in its as-grown state, where no scattering is visible at the half-integer positions, with data taken after reduction, which reveal weak peaks at the half-integer positions. This sample was reduced at a lower temperature (890 °C compared to 960–970 °C for the Ce-doped samples), because undoped samples completely decompose after being reduced at 960 °C. Note that the peaks here are approximately two orders of magnitude smaller than in the previous cases, resulting in an approximate $(Nd,Ce)_2O_3$ volume fraction of only 0.02%.

Our x-ray diffraction results are consistent with an earlier study that only reported the existence of only one class of additional peaks ("$L=$even" peaks in Fig. 7) from scans at $L=0$.[28] However, the appearance of these additional peaks was attributed to coherent atomic displacements of NCCO rather than to the $(Nd,Ce)_2O_3$ secondary phase. Interestingly, this study also reports that the additional peaks disappear upon oxygenation of reduced samples, suggesting that the formation of the secondary phase is a reversible process. Finally, we note that another study reported epitaxial inclusions of Cu_2O in $Nd_2CuO_{4+\delta}$ samples grown via the flux method in high excess amounts of CuO flux.[36] To date, we have not found any evidence for such a phase in our crystals.

VII. TRANSMISSION ELECTRON MICROSCOPY

To confirm our diffraction results with real-space information, we used transmission electron microscopy (TEM) to characterize the microstructure of a reduced $x=0.16$ crystal. A small section of the crystal was prepared with a [0,1,0]

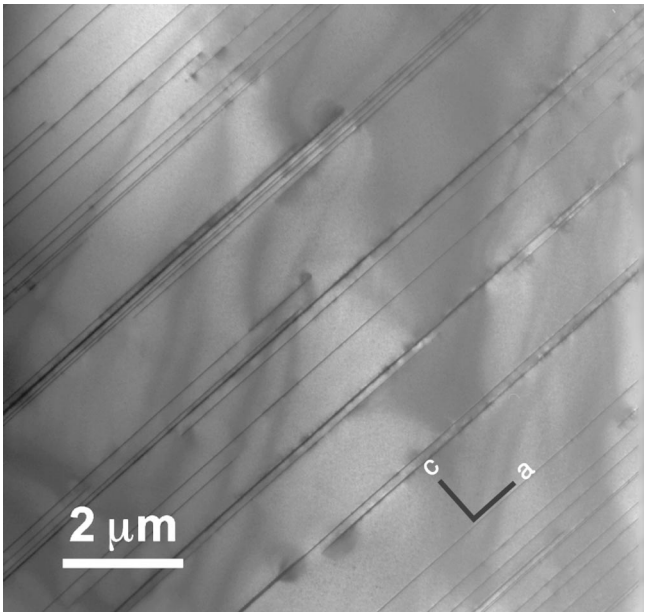

FIG. 10. Medium-resolution [0,1,0] TEM image of a reduced $x=0.16$ sample (NCCO16; see Table I) with layers of the $(Nd,Ce)_2O_3$ phase perpendicular to [0,0,1].

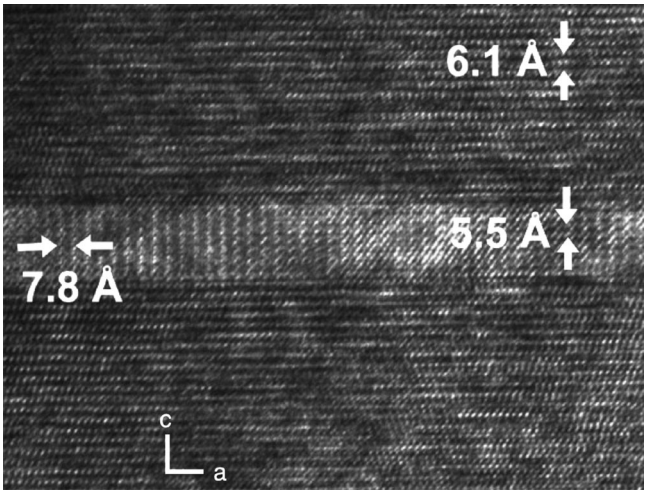

FIG. 11. High-resolution TEM image of the same crystal as in the previous figure with a secondary phase region, showing the epitaxial orientation of $(Nd,Ce)_2O_3$ in the NCCO matrix. The 6.1 Å $(0,0,2)$ planes of the matrix are parallel to the 5.5 Å $(0,0,2)_c$ planes of the secondary phase. The 7.8 Å perpendicular spacing for the secondary phase represents the $(1,1,0)_c$ planes, which are parallel to the $(0,2,0)$ planes of the matrix.

surface. A small piece was cut from the interior of the bulk sample, ground and polished from both sides (with diamond film paper) to a thickness of about 25 μm, mounted on a Cu support slot grid, and ion milled from both sides until perforation. The ion-milled hole was about 200 μm in diameter, and the sample was observed to have the same morphology in all thin areas around the edges of the hole, i.e., an area of about 250 μm in diameter and up to $\sim$1000 Å in thickness. It is important to note that electrons are transmitted directly through the sample such that at any point in the image one is measuring the entire thickness of the sample at that point. In regions far away from the perforation, the thickness of the sample is large so that there is no longer sufficient elastic transmission of the electrons to form an image.

Figure 10 shows an image that reveals thin straight layers of the secondary phase perpendicular to [0,0,1] of NCCO. The secondary-phase regions have a spatial extent well above 1 μm parallel to the CuO_2 planes of NCCO, i.e., perpendicular to [0,0,1]. In Fig. 11, we show a high-resolution image of a secondary-phase layer. $(Nd,Ce)_2O_3$ has an epitaxial relationship with the tetragonal NCCO matrix of $[0,0,1]_c \| [0,0,1]$ and $[1,1,0]_c \| [100]$. The extent of the $(Nd,Ce)_2O_3$ layers is minimized in the direction of greatest mismatch, i.e., along the *c*-axis of NCCO. While there are some rare regions as thick as 150 Å and some regions thinner than 40 Å, by averaging over 40 $(Nd,Ce)_2O_3$ layers identified on a series of photographs which spanned different regions of the sample, we estimate that the typical thickness is 60 Å. Again using information from several images such as that of Fig. 10, we arrive at a crude estimate of a secondary phase volume fraction of 1–3%. These estimates are in good agreement with our diffraction results listed in Table I.

We emphasize that in order to achieve the desired crystallographic orientation the measured piece was cut out from the interior of a much larger crystal, and that the electrons are probing the entire sample thickness. Consequently, TEM should not be considered a "local" or "surface" probe. In fact, our TEM results are remarkably consistent with the conclusions we have drawn from our x-ray diffraction data, and provide compelling, visual evidence of the unusual morphology of the secondary phase.

VIII. MAGNETIC FIELD EFFECTS

Having established the presence of $(Nd,Ce)_2O_3$ as a result of the partial decomposition of the NCCO matrix during reduction, we now investigate how this secondary phase responds to the application of a magnetic field. This is important because peaks from the secondary phase are found at positions associated with the two-dimensional antiferromagnetic zone center of NCCO. Therefore, it is essential to know how $(Nd,Ce)_2O_3$ responds to a field in order to avoid confusion between intrinsic and extrinsic effects when investigating the connection between magnetism and superconductivity in NCCO.

For this purpose, we placed a reduced, superconducting sample (NCCO18) in the horizontal-field magnet M2 at Chalk River Laboratories (Ontario, Canada). The sample was 1.6 cm long, 3.6 mm in diameter, and weighed 1.28 g. Because of a large easy-plane anisotropy for magnetic neodymium atoms in NCCO, the application of a magnetic field along [0,0,1] exerts a torque on the sample that attempts to twist it until the copper-oxygen planes are oriented parallel to the field direction. To counteract this, opposite faces of the sample perpendicular to [0,0,1] were ground flat and placed into a press-shaped sample mount. The sample was held fast in the mount by tightening the mount with screws against the flat sections of the crystal.

At zero field, some peaks from the secondary phase are visible. By comparing the integrated intensities of the

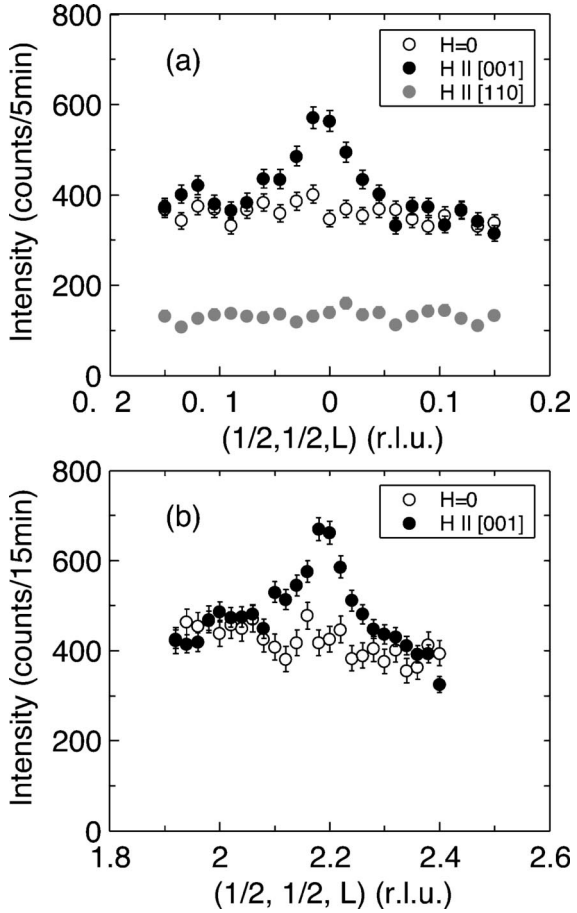

FIG. 12. *L*-scans through (a) (1/2,1/2,0) and (b) (1/2,1/2,2.2). The magnetic field strength is either 0 or 2.6 T. The sample is a $x=0.18$ crystal (NCCO18; see Table I). The data were taken at Chalk River Laboratories (Ontario, Canada) at a temperature of 2 K.

$(4,0,4)_c$ reflection of $(Nd,Ce)_2O_3$ [the (1,1,4.4) reflection in the NCCO reciprocal space] to the (0,0,2) and (0,0,4) reflections of NCCO, we estimate the volume fraction of the secondary phase to be approximately 0.5% in this sample.

In Fig. 12(a), we present *L*-scans through the (1/2,1/2,0) reflection, also indexable as $(2,0,0)_c$. This position is associated with the antiferromagnetic wave vector of the CuO_2 plane. Weak reflections are not always easily visible in neutron measurements due to the relatively low flux of neutron sources when compared to x-ray synchrotrons as well as the relatively high background scattering and coarse momentum resolution in neutron scattering experiments. In the present case, no peak can be discerned above background at zero field, as expected, given the relatively small sample size and secondary phase volume fraction when compared to our $x=0.10$ sample for which we do observe a weak structural peak [Fig. 13(a)]. With the application of a magnetic field of 2.6 T directed along [0,0,1], perpendicular to the copper oxide planes, a peak is readily visible. In Fig. 12(b), we present a similar set of scans through the position (1/2,1/2,2.2), or $(2,0,2)_c$. As in the case of the $(2,0,0)_c$ reflection, no peak is visible at zero field, but upon application of a 2.6 T magnetic field directed along [0,0,1], a peak clearly emerges at $L=2.2$.

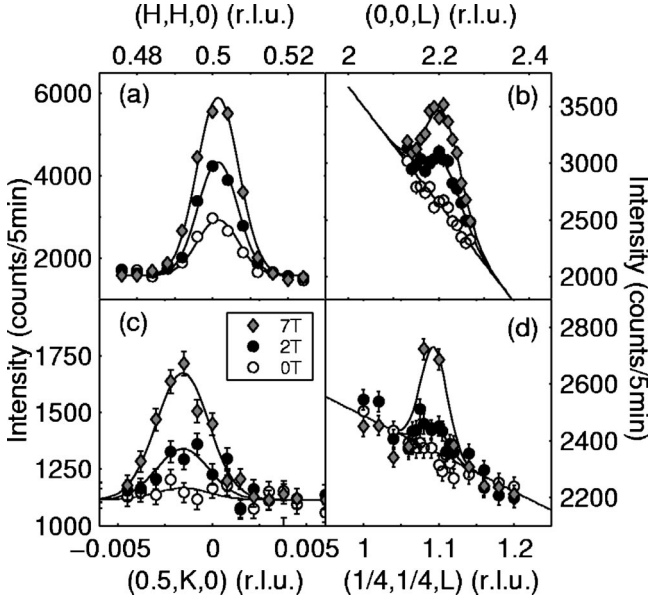

FIG. 13. Magnetic neutron diffraction scans at $T=4.2$ K for a reduced but *nonsuperconducting* sample (NCCO10; see Table I). In all cases, care was taken to ensure that the magnetic field was applied along a $\{1,0,0\}$ $(Nd,Ce)_2O_3$ axis and perpendicular to the scattering wave vector. Only scan (b) was originally taken at 5 min/point. All other scans were normalized to 5 min/point for clarity. (a), (b) Scans through (1/2,1/2,0) $[(2,0,0)_c]$ and the cubic-equivalent position (0,0,2.2) $[(0,0,2)_c]$. (c), (d) Scans through (1/2,0,0) $[(1,1,0)_c]$ and the cubic-equivalent position (1/4,1/4,1.1) $[(1,0,1)_c]$. The large sloping background for the (0,0,2.2) and (1/4,1/4,1.1) reflections results from the close proximity to, respectively, the strong NCCO (0,0,2) Bragg reflection and the direct beam at (0,0,0). This prohibits the observation of zero-field $(Nd,Ce)_2O_3$ structural scattering. However, from Gaussian fits of the field-induced data (solid lines) we extract a typical thickness of 115 Å, consistent with the structural results reported in Table I. The data were taken at the NIST Center for Neutron Research (Gaithersburg, MD, USA).

From the extensive x-ray survey of Sec. VI, we know that these two positions are associated with structural peaks of a secondary decomposition phase of $(Nd,Ce)_2O_3$. The application of a magnetic field polarizes the Nd moments of the secondary phase, which results in a ferromagnetic component that enhances the scattering at nuclear positions of the secondary phase, and renders the $(2,0,0)_c$ and $(2,0,2)_c$ peaks visible. This point is well demonstrated by Fig. 12(b), since the position (1/2,1/2,2.2) is manifestly unrelated to the NCCO structure. We test the proposition that the field-induced magnetism is ferromagnetic in nature by studying the effect of a 2.6 T field along [1,1,0] for scattering at the (1/2,1/2,0) position. As can be seen from Fig. 12(a), we find that a peak is no longer visible. This is due the geometric factor $S_\perp \equiv |\hat{\mathbf{Q}}\times(\mathbf{S}\times\hat{\mathbf{Q}})|$ in the magnetic neutron scattering cross-section for unpolarized neutrons[37]

$$\frac{d\sigma}{d\Omega_f} = N\frac{(2\pi)^3}{V}\left|\sum_j\left(\frac{g\gamma r_0}{2}\right)S_\perp e^{i\mathbf{Q}\cdot\mathbf{r}_j}\right|^2, \qquad (1)$$

which implies that the observed intensity is proportional to the square of the component of the moment perpendicular to

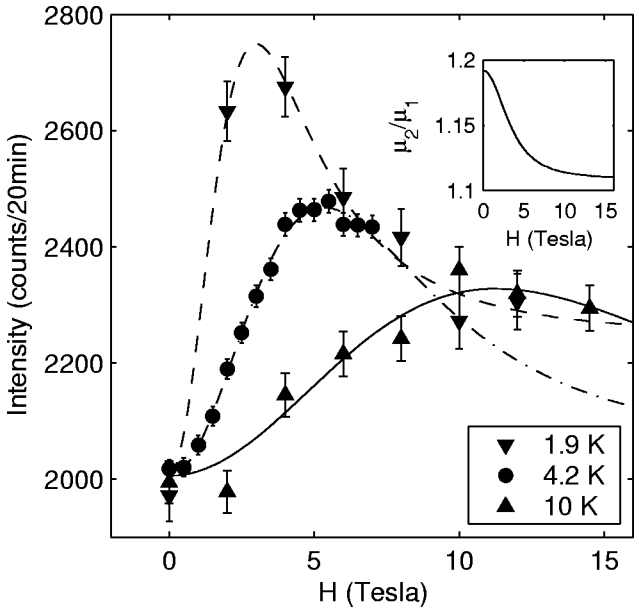

FIG. 14. Field dependence of the scattering observed at (1/2, 1/2,0) at several temperatures for a reduced $x=0.18$ sample (NCCO18; see Table I). The magnetic field was applied along [0,0,1]. The lines are the result of a fit to a two-moment model, as described in the text. (Inset) The ratio of the moment at the Nd(2) site to that at the Nd(1) site of $(Nd,Ce)_2O_3$ at 1.9 K, as extracted from the fit.

Q. Here, N is the number of unit cells, V is the volume of one unit cell, g is the Landé factor, γ is the gyromagnetic ratio, r_0 is the classical electron radius, and $\mathbf{r}_j$ are the atomic positions in the unit cell. Because the Nd moments are field-induced, their direction tends to follow the direction of the applied field. Neglecting possible small anisotropy effects, when the magnetic field is oriented along [0,0,1], the moment is perpendicular to the scattering wave-vector $\mathbf{Q}=(1/2,1/2,0)$, and the maximum contribution is obtained. However, when the field is directed along [1,1,0], the moments are parallel to the field, and hence parallel to $\mathbf{Q}=(1/2,1/2,0)$. In this geometry, the magnetic contribution to the scattering is zero and no peak can be distinguished. The increased background level in some scan geometries occurs for a narrow region of the magnet where the electrical wiring and cryogenic tubing is located, which leads to higher incoherent scattering than neighboring parts of the magnet when illuminated by the incident neutron beam.

Since the field-induced scattering originates from the secondary decomposition phase, it is observed in reduced samples, but not in as-grown samples. The oxygen-reduction procedure, which precipitates the secondary phase, is necessary to induce superconductivity. Thus, the fact that the field-induced scattering is seen in superconducting samples but not in nonsuperconducting samples does not imply that the observed field effect is related to superconductivity in the NCCO matrix. To demonstrate this, Fig. 13 shows magnetic scattering in an oxygen-reduced, nonsuperconducting NCCO crystal ($x=0.10$). The sample measured 4 mm in diameter, 2.1 cm in length, and weighed 3.5 g. The sample volume, the volume fraction of the secondary phase ($\sim 2\%$), and the neutron flux are larger than in the case of the $x=0.18$ sample. As a result, a structural peak is visible at (1/2,1/2,0) [i.e., $(2,0,0)_c$] in zero field. We also demonstrate enhanced scattering in a magnetic field at the equivalent position (0,0,2.2) [i.e., $(0,0,2)_c$]. We conclude that an enhancement of scattering in a magnetic field is observable in reduced NCCO, *irrespective* of whether or not the sample is superconducting. Furthermore, the effect is observable at any position corresponding to a structural reflection of the secondary $(Nd,Ce)_2O_3$ phase, subject, of course, to the modulation of the structure factor and the geometric factor $S_\perp^2$.

An important point to note about the bixbyite structure is that even in its most symmetric cubic form ($Ia3$) it is not a primitive unit cell, but has two crystallographically and magnetically distinct rare earth sites, as discussed in Sec. V. These two distinct magnetic sites can have very different magnetic moments, as is the case for Yb_2O_3.[24] Since the separate contributions to the structure factor from each site add destructively for some reflections, the observed intensity for a given reflection is a function of the relative strength of the magnetic moments on the two sites. For cubic Nd_2O_3, the magnetic structure factor of the $(2,0,0)_c$ reflection is proportional to

$$F(2,0,0)_c \sim |-8\mu_1 + 7.39\mu_2|, \tag{2}$$

where the two contributions come from the two inequivalent neodymium sites with potentially inequivalent moments. Because of the negative phase between the two contributions, in the case of identical moments there is a 92% cancelation between the contributions from the two sites. Since the atoms with C_2 symmetry are slightly displaced from the cell edge, the cancelation is incomplete. This also holds for nuclear scattering, in which case μ is replaced by the scattering length b_{Nd}. For the $(2,0,2)_c$ reflection, the structure factor is proportional to

$$F(2,0,2)_c \sim |8\mu_1 - 8\mu_2|. \tag{3}$$

Assuming cubic symmetry, the non-zero intensity apparent in Fig. 12(b) then implies that the magnetic moments on the two Nd sites are different for this particular field and temperature. Furthermore, the existence of inequivalent moments implies that the evolution of the magnetic moment with field is also slightly different between the two sites. As a result, a nontrivial field dependence of the scattering intensity may be observed.

In Fig. 14, we show the field dependence of the scattering at (1/2,1/2,0) for the NCCO ($x=0.18$) sample at three different temperatures. The lowest and highest temperature data were taken using the two-axis diffractometer E4 at the Hahn-Meitner-Institut (Berlin, Germany) and the 4.2 K data were taken using the BT2 spectrometer at the NIST Center for Neutron Research (Gaithersburg, MD, USA). Temperature scans taken at constant field (data not shown) were used to cross-normalize the data sets taken at the two facilities. Both experiments employed a vertical-field magnet with field directed along [0,0,1], but the magnetic field range of the 4.2 K data set was limited by the 7 T maximum field of the

NIST magnet. We model the behavior illustrated in Fig. 14 by assuming that the moment on each Nd site evolves according to its own Brillouin function[38]

$$\mu_{1,2} = g\mu_B J_{1,2} B_{J_{1,2}},$$

$$B_J = \frac{J+1/2}{J}\coth[(J+1/2)\eta] - \frac{1}{2J}\coth(\eta/2),$$

$$\eta = \frac{g\mu_B H}{k_B T}, \tag{4}$$

and then combine the associated scattering intensity according to the aforementioned structure factor in Eq. (2). The effect of the crystal field on the total angular momentum J is unknown for $(Nd,Ce)_2O_3$, and we have fitted J at each temperature for both Nd sites. Once we fix the nonmagnetic scattering to 2000 counts/20 min., the fit involves an overall (temperature-independent) scale factor and two additional parameters per temperature: J_1 and J_2. From the lowest to highest temperature we find $J_1 = 2.1(2)$, 2.4(1), 2.6(2), and $J_2/J_1 = 1.110(4)$, 1.093(4), 1.085(4). The Landé factor g was fixed at the free ion value of 8/11 for Nd. Clearly, the two-moment model provides an excellent description of our data. In the inset of Fig. 14, we plot the field evolution of the ratio μ_2/μ_1 as extracted from the field dependence at the lowest temperature. Our model indicates that the saturated moments of the two sites differ by 11%. This observation is consistent with the 13% difference found for Er_2O_3 and the 77% difference found for Yb_2O_3.[24] From the fits, we estimate the low-temperature moment of the Nd(1) and Nd(2) atoms as $gJ\mu_B \approx 1.5\mu_B$ and $\approx 1.65\mu_B$, respectively. These are reasonable values, comparable to the experimentally observed value of $1.65\mu_B$ of cubic $NdNi_2$.[39] The two-moment model accounts not only for the complete field and temperature dependence of the scattering intensity, but also explains how what is essentially ferromagnetic scattering can decrease with increasing magnetic field.

The results presented in Fig. 14 indicate that $(Nd,Ce)_2O_3$ is paramagnetic even at 1.9 K. This is consistent with the fact that Er_2O_3 ($T_N = 3.4$ K) and Yb_2O_3 ($T_N = 2.3$ K) have relatively low Néel temperatures, and that the $(Nd,Ce)_2O_3$ secondary phase has a lower effective dimensionality. In a separate measurement we did not observe spontaneous Nd ordering (of $(Nd,Ce)_2O_3$ or NCCO) in our $x = 0.10$ sample down to 1.4 K.

A field-dependent peak was also observed at (1/2,0,0) [equivalent to $(1,1,0)_c$] and at (1/4,1/4,1.1) [equivalent to $(1,0,1)_c$], as demonstrated in Fig. 13. As discussed in Sec. VI, reflections at these positions are forbidden by the $Ia3$ glide-plane symmetry. Our observation of such peaks, together with the measured inequivalent *a*-*b* and *c* lattice constants of the secondary phase, are evidence of a lowered symmetry in the strained $(Nd,Ce)_2O_3$ environment inside the NCCO matrix. An analysis of the maximal crystallographic subgroups of $Ia3$ suggests that the symmetry is lowered by a positional shift of the Nd(2) atoms. Calculations show that the Nd(1) atoms do not contribute to the structure factor at $(1,1,0)_c$, and the contributions from the other Nd atoms [formerly Nd(2) atoms] add in phase. This suggests that the magnetic-field dependence at (1/2,0,0) [i.e., $(1,1,0)_c$] should saturate at sufficiently large magnetic fields. Although we were unable to reach high enough field values in order to test this prediction [c.f. Fig. 16(c)], recent results by another group are consistent with it.[13]

We note that the interpretation of the magnetic-field dependence at intrinsic magnetic reflections of NCCO is complicated by the expected polarization of the Nd atoms of NCCO and by remnant magnetic order in reduced samples. Antiferromagnetic reflections of NCCO, such as (1/2,3/2,0), have two contributions to the structure factor. One is from copper, and the other is from neodymium. The latter acquires an induced antiferromagnetic order due to the staggered magnetic field of the copper atoms below the copper ordering temperature. The two NCCO contributions can either be in-phase [e.g, (1/2,3/2,0), (1/2,1/2,3), and (1/2,1/2,6)] or out-of-phase [e.g., (1/2,1/2,1)], depending on the reflection. In zero applied magnetic field, the two contributions manifest themselves as a dramatic change in the scattering intensity at low temperatures when the Nd moments become appreciable.[40] In an applied magnetic field, Nd moments of NCCO will be polarized, which is clear from the quadratic increase of intensity observed at (1,1,0) in as-grown samples.[9,11,13] In reduced samples, in addition to the above effect in remnant antiferromagnetic regions of the sample, we can expect an additional contribution from $(Nd,Ce)_2O_3$ at reflections that coincide with those of NCCO, such as (1/2,3/2,0). The net effect depends on the temperature, the magnetic field strength, the geometry of the experiment, and the measured reflection.

Our field-effect results establish that a magnetic contribution from $(Nd,Ce)_2O_3$ is present at (1/2,1/2,0), the two-dimensional antiferromagnetic zone center of NCCO, and at equivalent positions, but they leave open the possibility that a small fraction of the signal may be intrinsic to the copper-oxygen sheets. One way to attempt to separate the two possible contributions is to perform scans at reciprocal space positions with nonzero, integer L, with a magnetic field along [0,0,1], such that the scattering from NCCO and from $(Nd,Ce)_2O_3$ is clearly separated. Experimentally, this requires that the sample be aligned in the (H,H,L) scattering zone and that a horizontal-field magnet be employed. Only a few such magnets compatible with use at a neutron diffractometer exist, and their maximum field is less than that of vertical-field magnets.

Figure 15 shows the result of such a measurement for a reduced $x = 0.18$ sample, performed at Chalk River Laboratories (Ontario, Canada) at three antiferromagnetic Bragg peak positions corresponding to $(1/2,1/2,L)$ with both even and odd integer values of L. As-grown NCCO exhibits long-range magnetic order of the copper moments even at high cerium concentrations, with Néel temperature $T_N \sim 80 - 100$ K for $x = 0.16 - 0.18$.[23] Along $(1/2,1/2,L)$, magnetic Bragg scattering is observed at non-zero integer values of L. The zero-field magnetic intensity at these positions in reduced, superconducting samples is relatively weak when compared to as-grown NCCO,[23,40,41] and the antiferromag-

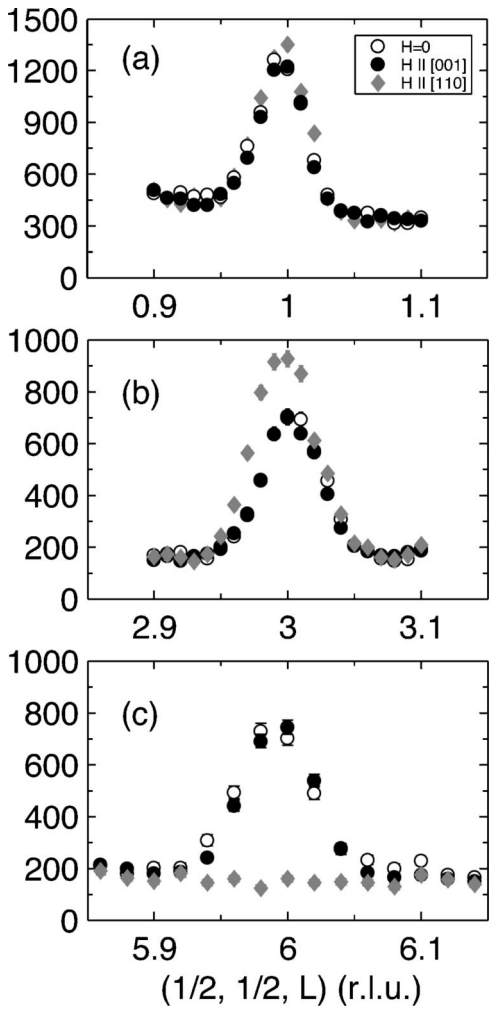

FIG. 15. Scans through NCCO magnetic peak positions $(1/2,1/2,L)$ for a reduced $x=0.18$ sample (NCCO18; see Table I). The magnetic field was 2.6 T. In (a) the temperature was 2 K and in (b) and (c) it was 5 K. The zero-field magnetic scattering only appears below 8 K. Whereas a magnetic field applied along the *c*-axis has no effect, an in-plane field along [1,1,0] slightly enhances the odd-integer-*L* peak and completely suppresses the even-integer-*L* scattering. The data were taken at Chalk River Laboratories (Ontario, Canada).

netic volume fraction rapidly decreases with increasing x in the superconducting phase.[42] Moreover, it has been found that the antiferromagnetic regions have a finite extent of 50–100 Å in superconducting samples with $x \geqslant 0.15$.[41] In our case ($x=0.18$), the scattering indeed is very weak, and only appears below ~8 K. From Fig. 15, we see that a [0,0,1] magnetic field has no net effect on the scattering intensity for both "in-phase" and "out-of-phase" reflections of the remnant NCCO antiferromagnetic regions. Since there is no observable effect for either class of reflection, we conclude that there is no evidence for a contribution from the bulk superconducting regions.

However, a field parallel to the copper-oxygen planes enhances the odd-*L* peak intensity and completely suppresses the even-*L* peak. Presumably this is the result of a noncollinear to collinear spin transformation similar to what has previously been reported,[43] but in the present case the orientation of the central spin (at the body-center position; see Fig. 1) is rotated by π resulting in the elimination of even-*L*, rather than odd-*L* peaks.

IX. DISCUSSION

Kang and coworkers reported magnetic-field-induced scattering at (1/2,1/2,0), (1/2,0,0) and related reflections, and interpreted their data as indicative of a field-induced quantum phase transition from a superconducting to an antiferromagnetic state.[9] In a previously published version of Fig. 16,[14] we demonstrated that a number of data sets taken at different temperatures, magnetic fields, reciprocal space positions, and on different samples (both superconducting and nonsuperconducting) could be scaled onto an approximately universal curve of scattering intensity versus H/T. We argued that these observations were inconsistent with a quantum phase transition from a superconducting to an antiferromagnetic state, and instead suggested that the data could be explained by a two-moment paramagnetic model for $(Nd,Ce)_2O_3$, introduced in detail in Sec. VIII.

Kang and coworkers now also observe $(Nd,Ce)_2O_3$ in their reduced samples and conclude that this secondary phase does indeed exhibit a field-induced paramagnetic response which leads to an enhancement of the scattering intensity at the reciprocal space positions they originally measured.[10,11,13] Matsuura *et al.* estimate the thickness of their secondary phase to be 220 Å, but argue that the secondary phase possess essentially three-dimensional long-range structural order.[13] Yet, our precise measurement of the lattice parameters of the secondary phase unequivocally shows that the structural symmetry of the bixbyite $(Nd,Ce)_2O_3$ phase is no higher than tetragonal. Further, we and Matsuura *et al.* observe intensities at reciprocal lattice positions forbidden by the glide-plane symmetry of the *Ia*3 space-group. Both these results clearly show that the structural symmetry of the secondary phase is much lower than *Ia*3, and therefore, its magnetic structure and response are likely to be even more complex than those predicted by the two-moment model discussed in Sec. VIII. This model should therefore be viewed as an effective description of the system.

The authors of Refs. 10, 11, and 13, argue that they have evidence for a NCCO contribution that can be effectively extracted by, for example, subtracting the intensity at (1/2, 1/2,0) $[(2,0,0)_c]$ measured with $\mathbf{H}\|[1,\bar{1},0]$ $([0,1,0]_c)$ from that measured with $\mathbf{H}\|[0,0,1]$ $([0,0,1]_c)$. In both geometries the scattering wave-vector $\mathbf{Q}$ is perpendicular to $\mathbf{H}$ and, under the assumption of cubic *Ia*3 symmetry and three-dimensional long-range order, the contribution from $(Nd,Ce)_2O_3$ should be the same.

This procedure was attempted in Refs. 12 and 13. In Fig. 17, we reproduce the difference data reported in Ref. 13. In addition, we reproduce the original, uncorrected data of Ref. 9 taken with a magnetic field along [0,0,1]. We note that although there is a reported difference in the magnitude of the scattering between the two geometries, the subtraction procedure does not alter the field dependence of the data. We

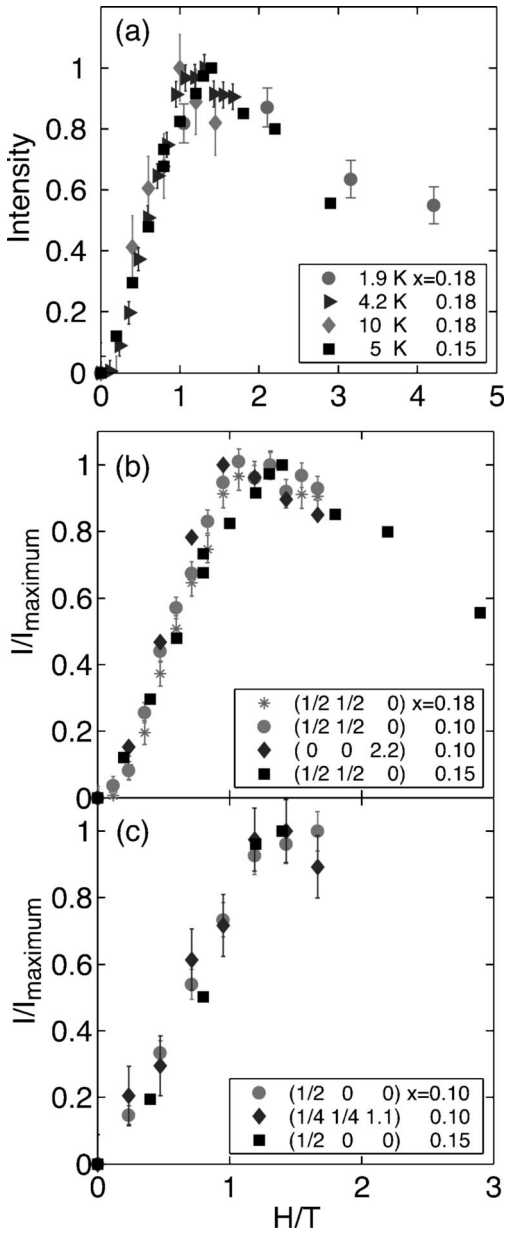

FIG. 16. Field and temperature dependence of magnetic scattering. (a) Arbitrarily scaled scattering intensity at (1/2,1/2,0) for a superconducting sample of NCCO (nominal cerium concentration $x=0.18$; $T_c=20$ K) at several temperatures, plotted as a function of H/T with the field along [0,0,1]. The results are compared with the data at $T=5$ K of Kang *et al.* [Ref. 9] ($x=0.15$; $T_c=25$ K). (b), (c) Comparison of the result by Kang *et al.* ($x=0.15$) with data taken at $T=4$ K for a superconducting sample ($x=0.18$) and a nonsuperconducting sample ($x=0.10$). The magnetic field is applied along $[1,\bar{1},0]$ for (0,0,2.2) and (1/4,1/4,1.1) and along [0,0,1] in all other cases. The data were normalized by the maximum intensity. Our samples are listed as NCCO10 and NCCO18 in Table I. This figure is reproduced from Ref. 14.

also show a fit of the uncorrected data of Ref. 9 to the two-moment paramagnetic model of Sec. VIII, and obtain $J_1=2.9(3)$ and $J_2/J_1=1.12(1)$. This fit describes the data just as well as the theoretical treatment for the SO(5) model of high-temperature superconductivity.[12] We emphasize that this fit gives results for the low-temperature moments and the ratio J_2/J_1 that are in excellent agreement with those extracted from our own data, and in very reasonable agreement with previous results for other rare earth oxides. Given that a quantum phase transition in NCCO and paramagnetism of $(Nd,Ce)_2O_3$ are fundamentally different physical phenomena, we consider it highly unlikely that the two should have the same magnetic field dependence, and hence conclude that the subtraction procedure is an unreliable means of correcting the data. This may be in part due to a thin-film-like magnetic anisotropy present in the secondary phase or to experimental difficulties in accurately normalizing the signal between the two geometries.

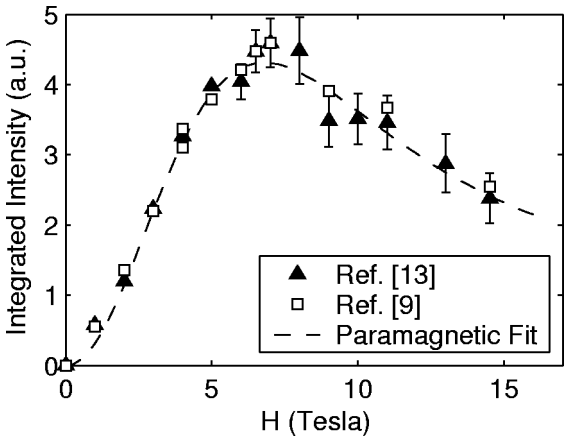

FIG. 17. Experimental results ($x=0.15$; $T=5$ K) for the field dependence of the normalized moment from Ref. 9 with $(Nd,Ce)_2O_3$ two-moment fit (dashed line), as described in the text. Also shown are the difference data from Ref. 13.

The only observation of Refs. 9 and 11 that differs from our own results is the field dependence of the (1/2,1/2,3) peak. As noted at the end of Sec. IX, the volume fraction of the NCCO antiferromagnetic phase strongly decreases with increasing cerium concentration in reduced samples. We note that the superconducting and antiferromagnetic volume fractions have been found to be highly anticorrelated.[42] Given the sample inhomogeneity issues discussed in Sec. IV, it appears likely that this (zero-field) magnetic response is due to a nonsuperconducting remnant of the as-grown state, with modified oxygen concentration and disorder. The response to a magnetic field of this remnant phase is *a priori* unclear, since the phase is altered by the oxygen treatment from the as-grown state. Our data taken in the horizontal-field geometry and presented in Fig. 15 do not indicate any change in the scattering at the (1/2,1/2,1), (1/2,1/2,3), and (1/2,1/2,6) reflections of NCCO for magnetic fields up to 2.6 T oriented along [0,0,1]. Given that a field of 2.6 T constitutes a significant fraction of the upper critical field in this geometry, the absence of a field effect suggests that the scattering at the reflections of the NCCO antiferromagnetic minority phase is unrelated to the suppression of superconductivity in the NCCO majority phase.

In Refs. 9 and 11, a small enhancement of the (1/2,1/2,3) intensity was reported in fields up to 4 T along [0,0,1], also

at 5 K, for a $x=0.15$ sample. The cerium concentrations of this sample is somewhat different from ours ($x=0.18$) and the effect of a magnetic field on the antiferromagnetic NCCO minority phase may have a subtle doping, temperature, and field dependence. Alternatively, since the Nd moment increases quite dramatically in a $1/T$ fashion, and because it contributes to the NCCO structure factor,[40] small temperature differences between two scans could, in principle, appear as a change in intensity. A third possible origin for the observed field effect reported in Refs. 9 and 11 could be due to the torque exerted on the sample for field configurations $\mathbf{H}\|[0,0,1]$. If the mount used in the experiment is not sufficiently rigid the sample may rotate, resulting in a difference in intensity between two scans. Considering our result reported in Fig. 15 in which a field directed along the [1,1,0] direction increases the amount of scattering at the (1/2,1/2,3) reflection, small changes in the alignment of the sample can either increase or decrease the observed scattering intensity. Finally, we note that the (1/2,1/2,3) data in Fig. 9(d) of Ref. 11 have relatively large error bars and are not entirely inconsistent with the absence of a field dependence.

An earlier study of $Nd_{2-x}Ce_xCuO_{4\pm\delta}$ ($x=0.14$) in [0,0,1] fields up to 10 T failed to detect any enhancement of the scattering intensity at the (1/2,3/2,0) reflection.[44] The lowest temperature at which data were taken in that experiment was a relatively high 15 K. Because of the strong enhancement of the Nd moment at low temperatures, this would have made detection of the effect from the $(Nd,Ce)_2O_3$ phase more difficult. Also, measurements were only conducted at the (1/2, 3/2,0) position. This is an allowed NCCO magnetic reflection, unlike (1/2,1/2,0), which is disallowed by the spin structure. Consequently, the additional contribution from $(Nd,Ce)_2O_3$ would also have been difficult to detect due to the prominence of the large signal from the NCCO antiferromagnetic phase regions of the sample, since the volume fraction of the remnant NCCO antiferromagnetic phase is still relatively large for $x=0.14$.[42] A subsequent experiment, conducted on the related electron-doped compound $Pr_{1-x}LaCe_xCuO_4$ (PLCCO) for $x=0.15$ ($T_c=16$ K), failed to detect any magnetic field effects at the (3/2,1/2,0) reflection in fields of up to 8.5 T along [0,0,1].[45] This is consistent with our observations. PLCCO has the advantage that La is a nonmagnetic ion, and the Pr moment is an order of magnitude weaker than that of Nd at low temperatures. Therefore, any complicating magnetic effects from a $(Pr,La,Ce)_2O_3$ secondary phase should be considerably weaker. The failure to observe a magnetic field effect deep inside the superconducting dome at $x=0.15$ is consistent with our conclusion that such effects in NCCO can be entirely accounted for by the $(Nd,Ce)_2O_3$ secondary phase. We note that some effects qualitatively different from those in NCCO were reported for an $x=0.11$ sample that lies on the boundary of the antiferromagnetic and superconducting regions of the $Pr_{1-x}LaCe_xCuO_4$ phase diagram.[45] It appears that those are attributable to a disturbance of the antiferromagnetic $Pr_{1-x}LaCe_xCuO_4$ minority phase and unconnected with superconductivity.

X. SUMMARY

In conclusion, we have observed that when $Nd_{2-x}Ce_xCuO_{4\pm\delta}$ is exposed to a reducing environment a fraction of the crystal decomposes. One of the decomposition products is $(Nd,Ce)_2O_3$, which precipitates epitaxially (on the CuO_2 planes of $Nd_{2-x}Ce_xCuO_{4\pm\delta}$) in a strained bixbyite structure. The structure is long-range correlated parallel to the copper-oxygen planes, but only short-range ordered perpendicular to the planes. Application of a magnetic field polarizes the Nd atoms, leading to an enhancement of the magnetic neutron scattering intensity at positions coincident with $(Nd,Ce)_2O_3$ structural peaks. A simple two-moment model for the $(Nd,Ce)_2O_3$ paramagnetism gives an excellent description of our data. The extensive data presented here are inconsistent with the notion[9–13] of a field-induced quantum phase transition from a superconducting to an antiferromagnetic ground state of $Nd_{2-x}Ce_xCuO_{4\pm\delta}$. In a recent neutron scattering experiment, it was observed that the antiferromagnetic fluctuations at the wave-vector (1/2,1/2,0) become gapped in the superconducting state.[46] The gap might only gradually close in a magnetic field, and for fields larger than H_{c2}, the ground state may not exhibit long-range antiferromagnetic order. Clearly, it will be important to test this possibility in future experiments. Finally, we note that the presence of the secondary phase should also be taken into account in the analysis of other experiments on $Nd_{2-x}Ce_xCuO_{4\pm\delta}$, such as transport measurements.

ACKNOWLEDGMENTS

The authors would like to thank N. Kaneko for his efforts in constructing the reduction furnace and maintaining the crystal growth facility at Stanford University, and A. Arvanitaki for assistance in orienting the TEM sample. The authors are also grateful for valuable comments by J.M. Tranquada, N.P. Armitage, H. Eisaki, E.M. Motoyama, T.W. Klimczuk, and D. Petitgrand. The authors would like to thank J.W. Lynn for technical assistance with the neutron scattering measurements at NIST. Finally, the authors wish to acknowledge P. Dai, H.J. Kang, J.W. Lynn, M. Matsuura, and S.C. Zhang for discussing their data with us. SSRL is supported by the DOE Office of Basic Energy Sciences, Division of Chemical Sciences and Materials Sciences. The work at Stanford University was furthermore supported by the U.S. Department of Energy under Contracts No. DE-FG03-99ER45773 and No. DE-AC03-76SF00515, and by NSF CAREER Award No. DMR9985067.

*Present address: Department of Physics, University of Toronto, Toronto, Ontario M5S 1A7, Canada.
†Present address: NIST Center for Neutron Research, National Institute of Standards and Technology, Gaithersburg, Maryland 20899.

[1] S. Katano, M. Sato, K. Yamada, T. Suzuki, and T. Fukase, Phys. Rev. B **62**, R14677 (2000).
[2] B. Lake, G. Aeppli, K. N. Clausen, D. F. McMorrow, K. Lefmann, N. E. Hussey, N. Mangkorntong, M. Nohara, H. Takagi, T. E. Mason, and A. Schröder, Science **291**, 1759 (2001).
[3] B. Lake, H. M. Ronnow, N. B. Christensen, G. Aeppli, K. Lefmann, D. F. McMorrow, P. Vorderwisch, P. Smeibidl, N. Mangkorntong, T. Sasagawa, M. Nohara, H. Takagi, and T. E. Mason, Nature (London) **415**, 299 (2002).
[4] B. Khaykovich, R. J. Birgeneau, F. C. Chou, R. W. Erwin, M. A. Kastner, S.-H. Lee, Y. S. Lee, P. Smeibidl, P. Vorderwisch, and S. Wakimoto, Phys. Rev. B **67**, 054501 (2000).
[5] E. Demler, S. Sachdev, and Y. Zhang, Phys. Rev. Lett. **87**, 067202 (2001).
[6] P. Fournier, P. Mohanty, E. Maiser, S. Darzens, T. Venkatesan, C. J. Lobb, G. Czjzek, R. A. Webb, and R. L. Greene, Phys. Rev. Lett. **81**, 4720 (1998).
[7] Y. Wang, S. Ono, Y. Onose, G. Gu, Y. Ando, Y. Tokura, S. Uchida, and N. P. Ong, Science **299**, 86 (2003).
[8] Y. Tokura, H. Takagi, and S. Uchida, Nature (London) **337**, 345 (1989).
[9] H. J. Kang, P. Dai, J. W. Lynn, M. Matsuura, J. R. Thompson, S. C. Zhang, D. N. Argyriou, Y. Onose, and Y. Tokura, Nature (London) **423**, 522 (2003).
[10] H. J. Kang, P. Dai, J. W. Lynn, M. Matsuura, J. R. Thompson, S. C. Zhang, D. N. Argyriou, Y. Onose, and Y. Tokura, Nature (London) **426**, 140 (2003).
[11] M. Matsuura, P. Dai, H. J. Kang, J. W. Lynn, D. N. Argyriou, K. Prokes, Y. Onose, and Y. Tokura, Phys. Rev. B **68**, 144503 (2003).
[12] H. D. Chen, C. Wu, and S. C. Zhang, Phys. Rev. Lett. **92**, 107002 (2004).
[13] M. Matsuura, P. Dai, H. J. Kang, J. W. Lynn, D. N. Argyriou, Y. Onose, and Y. Tokura, Phys. Rev. B **69**, 104510 (2004).
[14] P. K. Mang, S. Larochelle, and M. Greven, Nature (London) **426**, 139 (2003).
[15] P. G. Radaelli, J. D. Jorgensen, A. J. Schultz, J. L. Peng, and R. L. Greene, Phys. Rev. B **49**, 15322 (1994).
[16] A. Manthiram and J. B. Goodenough, J. Solid State Chem. **87**, 402 (1990).
[17] J. A. McAllister, S. Davies, and J. P. Attfield, J. Solid State Chem. **155**, 138 (2000).
[18] J. F. Bringley, S. S. Trail, and B. A. Scott, J. Solid State Chem. **86**, 310 (1990).
[19] *Nonstoichiometric Oxides*, edited by O. T. Sørensen (Academic Press, New York, 1981).
[20] A. J. Schultz, J. D. Jorgensen, J. L. Peng, and R. L. Greene, Phys. Rev. B **53**, 5157 (1996).
[21] J. M. Tarascon, E. Wang, L. H. Greene, R. Ramesh, B. G. Bagley, G. W. Hull, P. F. Miceli, Z. Z. Wang, D. Brawner, and N. P. Ong, Physica C **162**, 285 (1989).
[22] A. Nath, N. S. Kopeleve, V. Chechersky, J. L. Peng, R. L. Greene, O. Beom-hoan, M. I. Larkin, and J. T. Markert, Science **265**, 73 (1994).
[23] P. K. Mang, O. P. Vajk, A. Arvanitaki, J. W. Lynn, and M. Greven, Phys. Rev. Lett. **93**, 027002 (2004).
[24] R. M. Moon, W. C. Koehler, H. R. Child, and L. J. Raubenheimer, Phys. Rev. **176**, 722 (1968).
[25] In previous publications we reported the furnace control temperature instead of the sample temperature.
[26] J. S. Kim and D. R. Gaskell, Physica C **209**, 381 (1993).
[27] In our original publication (Ref. 14) we gave an estimate of 0.01–0.1% for the typical secondary phase volume fraction. Table I contains refined estimates, ranging two orders in magnitude, from ~0.02 to ~2%, depending on the reduction conditions.
[28] K. Kurahashi, H. Matsushita, M. Fujita, and K. Yamada, J. Phys. Soc. Jpn. **71**, 910 (2002).
[29] M. Brinkmann, T. Rex, H. Bach, and K. Westerholt, Phys. Rev. Lett. **74**, 4927 (1995).
[30] G. Adachi and N. Imanaka, Chem. Rev. (Washington, D.C.) **98**, 1479 (1998).
[31] R. W. G. Wyckoff, *Crystal Structures*, Vol. 1, 2nd ed., Chapt. V (Interscience Publishers, New York, 1963).
[32] T. Hahn, ed., *International Tables for Crystallography*, Vol. A (Kluwer Academic, Dordrecht, The Netherlands, 2002).
[33] F. Izumi, Y. Matsui, H. Takagi, S. Uchida, Y. Tokura, and H. Asano, Physica C **158**, 433 (1989).
[34] B. E. Warren, *X-Ray Diffraction* (Dover Publications, New York, 1990).
[35] A. Gibaud, R. A. Cowley, D. F. McMorrow, R. C. C. Ward, and M. R. Wells, Phys. Rev. B **48**, 14463 (1993).
[36] P. Galez, P. Schweiss, G. Collin, and R. Belissent, J. Less-Common Met. **164**, 784 (1990).
[37] G. Shirane, S. M. Shapiro, and J. M. Tranquada, *Neutron Scattering with a Triple-Axis Spectrometer* (Cambridge University, Cambridge, England, 2002).
[38] C. Kittel, *Introduction to Solid State Physics*, 7th ed. (Wiley, New York, 1996).
[39] E. A. Skrabek and W. E. Wallace, J. Appl. Phys. **34**, 1356 (1963).
[40] M. Matsuda, Y. Endoh, K. Yamada, H. Kojima, I. Tanaka, R. J. Birgeneau, M. A. Kastner, and G. Shirane, Phys. Rev. B **45**, 12548 (1992).
[41] T. Uefuji, K. Kurahashi, M. Fujita, M. Matsuda, and K. Yamada, Physica C **378–381**, 273 (2002).
[42] T. Uefuji, T. Kubo, K. Yamada, M. Fujita, K. Kurasashi, I. Watanabe, and K. Nagamine, Physica C **357–360**, 273 (2001).
[43] S. Skanthakumar, J. W. Lynn, J. L. Peng, and Z. Y. Li, Phys. Rev. B **47**, 6173 (1993).
[44] M. Matsuda, S. Katano, T. Uefuji, M. Fujita, and K. Yamada, Phys. Rev. B **66**, 172509 (2002).
[45] M. Fujita, M. Matsuda, S. Katano and K. Yamada, cond-mat/0311269 (unpublished).
[46] K. Yamada, K. Kurahashi, T. Uefuji, M. Fujita, S. Park, S. H. Lee, and Y. Endoh, Phys. Rev. Lett. **90**, 137004 (2003).